Macromolecules

ARTICLE

pubs.acs.org/Macromolecules

Effects of PEGylation on the Size and Internal Structure of Dendrimers: Self-Penetration of Long PEG Chains into the Dendrimer Core

Hwankyu Lee*,† and Ronald G. Larson‡

†Department of Chemical Engineering, Dankook University, Yongin 448-701, South Korea

‡Department of Chemical Engineering, Biomedical Engineering, Mechanical Engineering, and Macromolecular Science and Engineering Program, University of Michigan, Ann Arbor, Michigan 48109, United States

ABSTRACT: G4 PAMAM dendrimers grafted with poly(ethylene glycol) (PEG) of different sizes (M_w = 550 and 5000) and grafting densities (12−94% of surface terminals) were simulated using the coarse-grained (CG) force fields previously developed and reparametrized in this work. Simulations are carried out for G4, G5, and G7 un-PEGylated dendrimers that are either unprotonated, terminally protonated, or protonated on both terminals and interior sites, corresponding to pH values of >10, 7, and <5, respectively. As protonation increases, simulations show only a small (∼6% for G4 and G5) change of dendrimer radius of gyration R_g and show a structural transition from dense-core to dense-shell structure, both of which are in agreement with recent scattering experiments and all-atom simulations. For the PEGylated dendrimers, the R_g of the fully PEG(M_w = 5000)-grafted dendrimer also agrees well with experiment. Longer PEG chains with higher grafting density yield PEG−PEG crowding, which stretches dendrimer terminals toward water more strongly, leading to larger size and a dense-shell structure of the dendrimer. Long PEG chains at high grafting densities also penetrate into the dendrimer core, while short ones do not, which might help explain the reduced encapsulation of hydrophobic compounds seen experimentally in dendrimers that are 75%-grafted with long PEG's (M_w = 5000). This reduced encapsulation for dendrimers with long grafted PEG's has previously been attributed to PEG-induced dendrimer aggregation, but this explanation is not consistent with our previous simulations which showed no aggregation even with long PEG's but is consistent with the new simulations reported here that show PEG penetration into the core of the dendrimer to which the PEG is attached.

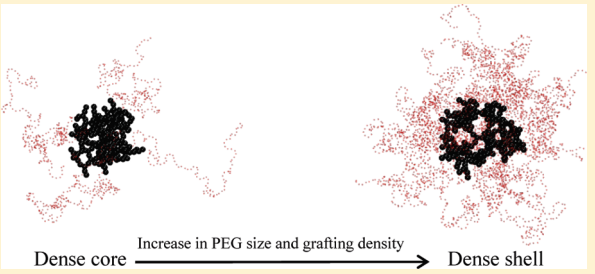

INTRODUCTION

Polyamidoamine (PAMAM) dendrimers are tree-branched polymers that have shown great potential for biomedical applications such as drug delivery and antitumor therapeutics because of their controlled size, uniform structure, surface functionality, and good water solubility.[1−9] For these applications, longer circulating lifetime, higher solubility, and lower cytotoxicity are required.[10,11] To achieve these properties, poly(ethylene glycol) (PEG) or poly(ethylene oxide) (PEO) is often attached to the dendrimer surface, a process called PEGylation. PEGylated PAMAM dendrimers have shown promise as gene vectors targeting brain, breast, and prostate cancers.[12−15]

As a step toward optimizing the size and concentration of PEGylated PAMAM dendrimers for these applications, the experiments of Kim et al. showed that relatively short PEG chains (M_w = 550, 750) with low grafting density (25% or less) significantly reduce the cytotoxicity of generation 3 (G3) PAMAM dendrimers, while maintaining their good water solubility.[16] Also, Yang et al. showed that grafting longer PEGs onto G3 PAMAM dendrimers increases their encapsulation of pyrene, a highly hydrophobic compound. However, dendrimers grafted with the longest PEG (M_w = 5000) showed reduced encapsulation of pyrene.[17] This nonmonotonic dependence of pyrene encapsulation on the length of the PEG has been interpreted as an indication that long PEG chains (M_w = 5000) may induce intermolecular aggregation of PEGylated dendrimers. The idea is that aggregation involves the interpenetration of long PEG chains into the neighboring dendrimers, thus occupying the other's interior and inhibiting encapsulation of pyrene into the dendrimer, reducing the ability of the PEGylated dendrimer to solubilize pyrene into water. However, our previous simulations showed no aggregation of long PEG (M_w = 5000)-conjugated G4 dendrimers,[18] which conflicts with the above interpretation of the experimental results. Therefore, the mechanism for nonmonotonic dependence of solubility on PEG length is still not understood. To resolve this, the internal structure of the PEGylated dendrimers needs to be studied at nearly the atomic scale for different PEG lengths. These atomic-scale interactions can be captured by molecular dynamics (MD) simulations, which have been successfully used to study other dendrimer systems such as the interaction with lipid bilayers.[19,20] Recently, Tanis and Karatasos performed MD simulations of a dendrimer attached to a single PEO chain to predict the conformation of the dendrimer and the hydrogen-bonding

Received: November 1, 2010
Revised: January 4, 2011
Published: March 10, 2011

dx.doi.org/10.1021/ma102482u | *Macromolecules* 2011, 44, 2291–2298

interaction between the dendrimer and PEO at various pH values.[21] Although this all-atom MD simulation study revealed atomic-scale details of the internal structure of PEGylated dendrimers, the simulation systems were limited to only a single PEO chain because of computational limitations on system size and time scale. Since in experiments multiple PEG/PEO chains are typically attached to each dendrimer, larger systems need to be simulated and for longer times. This can be done by using coarse-grained (CG) MD simulations, assuming that the CG force field can replicate the conformations and internal structures obtained in experiments and all-atom simulations. Previously, CG MD simulations successfully captured the conformation and internal structure of polyphenylene dendrimers in the melt,[22] and the effect of the PAMAM−dendrimer properties on the interaction with lipid bilayers,[23−26] with results in agreement with experimental results and all-atom simulations.

In this work, we therefore perform CG MD simulations of PEGylated G4 dendrimers with different lengths and grafting densities. First, to accommodate the effect of pH, we develop a reparametrized CG dendrimer force field and validate it by comparing predicted radius of gyration (R_g) values of un-PEGylated G4, G5, and G7 dendrimers at different pH with values from recent experiments and from all-atom simulations. Second, the conformations of the G4 dendrimer−PEG complexes and their PEG chains as well as diffusivities of the complexes are calculated and correlated with the PEG length and grafting density. Finally, the effect of the PEG length and grafting density on size and internal structure of the dendrimer is investigated and found to compare favorably with experimental results. In particular, we observe self-penetration of PEG chains into their own dendrimer core as a function of PEG lengths and grafting density. These findings can explain the experimentally observed nonmonotonic effect of PEG length on encapsulation of hydrophobic compounds without invoking aggregation of dendrimers, which our previous simulations have shown is absent.

METHODS

All simulations and analyses were performed using the GROMACS4.5.1 simulation package[27,28] with the "MARTINI" CG force field (FF).[29,30] The previously developed CG dendrimer FF[23] is here reparametrized to represent the experimentally measured radii of gyration (R_g) and the computationally calculated internal structure of un-PEGylated dendrimers for pH in the range 4−10.[31,32] For PEG, we used the CG PEG FF previously parametrized to predict R_g, diffusivities, hydrodynamics, and the distributions of bond lengths, angles, dihedrals, and end-to-end distances, all of which were close to those from all-atom simulation and experiments.[33,34] The CG dendrimer-terminal and PEG beads were linked via the bond and angle potentials for the CG PEG FF, and the Lennard-Jones (LJ) interactions between dendrimer and PEG were assigned by following the framework of the MARTINI model. A temperature of 298 K was maintained by applying a Berendsen thermostat in an NPT ensemble.[35] A cutoff of 12 Å was used for the LJ potential with a smooth shift to 0 between 9 and 12 Å. For the Coulomb potential, a short-range interaction with a cutoff of 12 Å and a long-range interaction with particle mesh Ewald summation[36] (PME) were used.

Parameterization and Equilibration of CG Dendrimers at Different pH Values. The electrostatic properties of PAMAM dendrimers are sensitive to pH. At high pH (>10), the dendrimer is not protonated, leading to a net dendrimer charge of 0, while the primary amines of the terminal groups of the dendrimer are protonated at neutral pH (∼7). Both the terminal primary amines and the inner tertiary amines are protonated at low pH (<5), leading to a high positive charge density.

We previously parametrized the CG dendrimer FF[23] by mapping dendrimer chemical moieties onto four different CG bead types within the framework of the MARTINI FF. Using this CG dendrimer FF, the R_g values of unacetylated G5 and G7 dendrimers (which contain cationic terminal charges at pH 7) were found to be close to experimental values.[23−26] Acetylated dendrimers (which are neutral and thus should have conformation similar to those of unacetylated dendrimers at high pH) had simulated R_g values that were ∼12% smaller than for unacetylated dendrimers, consistent with the results of other simulations and with theoretical calculations.[37−42] However, recent experimental results conflict with these findings. Chen et al. recently characterized the effect of pH on dendrimer conformation for G3−G8 dendrimers in water using both small-angle neutron scattering (SANS) and small-angle X-ray scattering (SAXS) with enhanced resolution.[31,43−46] They observed only small changes of the radii of gyration (R_g) of the dendrimer from high to low pH, conflicting with simulation predictions of a change in R_g of >12%.[37−42] These measurements also showed a strong interaction between counterions and protonated dendrimers at low pH, which suggests that the charges at low pH are heavily screened by counterions and that this suppresses the dendrimer swelling that would otherwise occur. Therefore, recently, the Goddard group reparametrized the nonbonding potentials for atoms within the dendrimer to strengthen the interactions between amines of the dendrimer and counterions. With this new FF, their all-atom MD simulations of protonated and unprotonated G4 dendrimers in water yielded only a small increase of R_g (∼5%) from high to low pH.[32] Also, analysis of radial distribution functions from their simulations showed dense-core structures at high pH and dense-shell structures at neutral and low pH. These recent experimental and simulation determinations of the conformation and internal structure of dendrimers at different pH values are good targets for CG simulations to predict.

To predict more accurately these dendrimer conformations at different pH values, we also reparameterized the LJ, bond, and angle potentials for the CG dendrimer model within the same mapping scheme that we used earlier. Figure 1 shows schematic pictures of a CG G1 PAMAM dendrimer at high (>10), neutral (∼7), and low pH (<5). For the LJ potential ($V_{LJ}(r_{ij}) = 4\varepsilon_{ij}[(\sigma_{ij}/r_{ij})^{12} - (\sigma_{ij}/r_{ij})^{6}]$, where σ_{ij} is bead diameter (Å) and ε is the well depth at the minimum (kJ/mol); $\varepsilon = 0$ for particles bonded to each other), bead types of "Qd" ($\varepsilon = 5.0$ and $\sigma = 4.7$; net charge of +1), "P3" ($\varepsilon = 5.0$ and $\sigma = 4.7$; no charge), and "N0" ($\varepsilon = 3.5$ and $\sigma = 4.7$; no charge) were used. Inner beads in the dendrimer are represented as either "Qd" or "N0", respectively, for the protonated ($NH^{+}-C_3H_6$) and unprotonated tertiary amines ($N-C_3H_6$). Each branch is represented by a "P3" bead for amides ($CH_2-CO-NH-CH_2$), which induces a stronger interaction with water (which is represented by "P4" beads) than does the bead "Nda" used for amides in our previous model. Note that the strong interaction between the amide and water has been observed in all-atom simulations.[47] In the standard MARTINI FF, $\varepsilon = 5.0$ and $\sigma = 4.7$ are assigned for the P3−P4 interaction, but here we use $\varepsilon = 5.1$ and $\sigma = 4.7$ to slightly increase the attractiveness between amide and water. For surface terminals, "Qd" or "P3" is used respectively for protonated

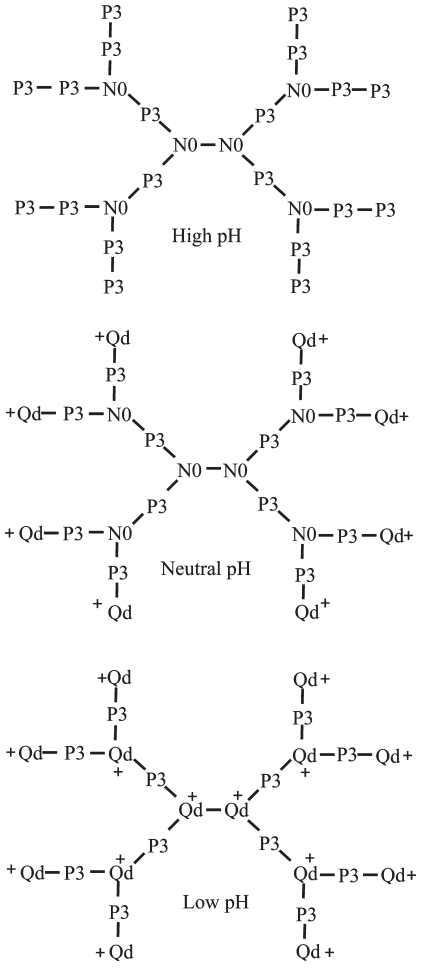

Figure 1. Schematic illustrations of the structure of the G1 dendrimer at high (>10; top), neutral (∼7; middle), and low pH (<5; bottom).

($CH_2NH_3^+$) and unprotonated primary amines (CH_2NH_2). For the bonding interaction, the bond length is controlled by the potential $V_{bond}(b) = {}^1/_2K_b(b - b_0)^2$, where K_b is the bond force constant (kJ $mol^{-1}nm^{-2}$), b is the instantaneous bond length (Å), and b_0 is the bond length at the minimum energy; for these we now take the new values $b_0 = 4.2$ and $K_b = 4000$. For the bond angle term $(V_{angle}(\theta) = {}^1/_2K_\theta(\cos(\theta) - \cos(\theta_0))^2$, where θ is the instantaneous bond angle (deg) and θ_0 is the bond angle at the minimum energy (kJ/mol)); new values $\theta_0 = 120$ and $K_\theta = 20$ are here used for inner node points (tertiary amines), and $\theta_0 = 160$ and $K_\theta = 70$ for the branches (amides).

Single CG G4, G5, and G7 dendrimers were solvated in periodic boxes of sizes 100, 120, and 135 Å/side, respectively. For each dendrimer generation, unprotonated, surface-protonated, and 100%-protonated dendrimers were simulated to represent their electrostatic properties at high, neutral, and low pH, respectively (Table 1). For a G4 dendrimer, ∼8800 water beads (equivalent to 35 200 waters) and 0, 64, or 126 Cl^- counterions were added at high, neutral, and low pH, respectively. For G5 and G7, ∼13 500 and ∼19 000 water beads were added with enough counterions to yield electroneutrality. Simulations were performed for 40 ns with a time step of 20 fs, and the last-10 ns trajectories were used for analyses.

Equilibration of CG PEGylated Dendrimers. 8, 16, 32, and 60 copies of PEG with M_w of 550 (PEG550) or 5000 (PEG5000) were attached to the surface terminals of G4 dendrimers obtained from the previous simulation equilibration runs. PEG chains were evenly distributed on the dendrimer surface. A PEG550- or PEG5000-attached dendrimer was solvated in 130 or 208 Å/side boxes, respectively, leading to ∼18 300 and ∼72 000 CG water beads. Since the linkage between dendrimer and PEG is an amide group, PEGylation neutralizes charges of the dendrimer terminal. Table 2 shows the numbers of charges for the dendrimer−PEG complexes, and counterions of 4−118 Cl^- were added to the systems to achieve electroneutrality. Simulations were performed for 400−500 ns with a time step of 8 fs. Analyses were performed with the first 100 ns deleted.

Table 1. Radii of Gyration (R_g) of G4, G5, and G7 Dendrimers at High, Neutral, and Low pH, Compared with Experiments

			R_g (Å)	
	pH	no. of charges	simulation	experiment[31]
G4	high		20.7 ± 0.1	21.4 ± 0.8
	neutral	64	21.7 ± 0.1	21.5 ± 0.5
	low	126	21.9 ± 0.1	21.6 ± 0.3
G5	high		25.7 ± 0.2	25.5 ± 0.6
	neutral	128	26.7 ± 0.1	26.9 ± 0.4
	low	254	27.3 ± 0.1	27.5 ± 0.4
G7	high		32.7 ± 0.2	34.1 ± 0.3
	neutral	512	35.0 ± 0.1	35.7 ± 0.2
	low	860	37.3 ± 0.1	36.7 ± 0.2

RESULTS AND DISCUSSION

Size and Internal Structure of Un-PEGylated Dendrimers at Different pH. To validate the reparametrized CG dendrimer FF, the size and internal structure of dendrimers at different pH values were calculated and compared with results from recent scattering experiments[31] and from all-atom simulations.[32] CG G4, G5, and G7 PAMAM dendrimers were unprotonated or protonated to mimic their electrostatic properties at pH values of 10 (high), 7 (neutral), and 4 (low) and simulated with water and counterions for 40 ns (Figure 1). Table 1 shows that the R_g values agree quantitatively with those obtained from recent SANS experiments.[31] Protonated dendrimers at low pH show a larger R_g than do unprotonated dendrimers at high pH, similar to experiments. The R_g values from simulations agree with those from experiments to within 4%. Also, from high to neutral pH, the R_g of a G5 dendrimer changes only 4%, in agreement with experiment, which is a more accurate prediction than obtained with our previous CG dendrimer FF.

Figure 2 shows radial density probabilities of G4 and G5 dendrimers as a function of distance from center of mass (COM) of the dendrimer. For the G4 dendrimer, a peak is found at around 9 Å at high and neutral pH. At neutral pH, a dip appears at around 7−8 Å, and at low pH the dip at 7−8 Å becomes more pronounced, and the peak shifts to 16−17 Å. These results indicate that the G4 dendrimer has a dense-core structure at high pH, since the monomer density has a maximum in the core with a decrease toward the edge but has a dense-shell structure at low pH, where there is a minimum at the core and an increase in monomer density toward the edge. A similar trend is observed for G5 and G7 dendrimers. These results are similar to those from

Table 2. Number of Charges per Dendrimer for G4 Dendrimers at High, Neutral, and Low pH, Attached with Different Lengths and Grafting Densities of PEG

		no. of charges	
pH	no. of PEG550 or PEG5000	tertiary amines (internal nodes)	primary amines (surface terminals)
high	8		
	16		
	32		
	60		
neutral	8		56
	16		48
	32		32
	60		4
low	8	62	56
	16	62	48
	32	62	32
	60	62	4

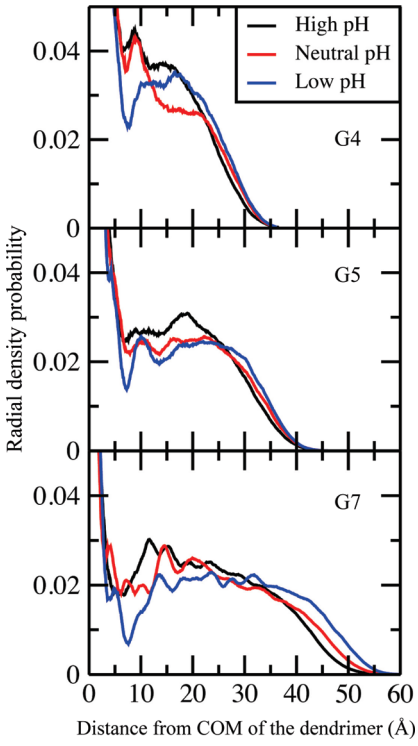

Figure 2. Radial density probabilites of all beads in the un-PEGylated dendrimer as a function of distance from center of mass (COM) of the dendrimer.

recent scattering experiments[31] and all-atom simulations,[32] indicating that the reparametrized CG dendrimer FF can capture the experimentally measured size and the computationally calculated internal structure of dendrimers at different levels of protonation and therefore at different pH values. In Figure 3, radial distribution functions (RDF) show that protonated amine groups of the dendrimer interact with counterions much more strongly than with water, supporting the conclusion that strong electrostatic interactions with ions significantly modulate the swelling of the

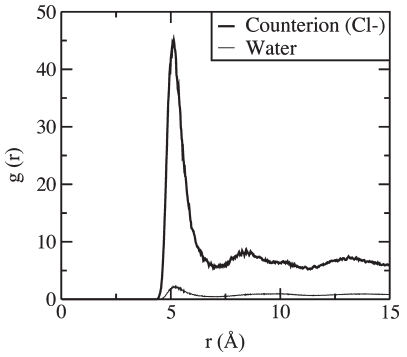

Figure 3. Radial distribution functions for counterions (Cl^-) and water with respect to protonated amines (dendrimer interior and terminals) of a G4 dendrimer.

dendrimer and internal structure, leading to a dense shell, as observed in all-atom simulations by the Goddard group.[32]

Conformation and Diffusivity of PEGylated Dendrimers. Differently protonated G4 dendrimers attached with 8, 16, 32, and 60 copies of PEG550 or PEG5000 were simulated for 400−500 ns (Table 2). Figure 4 shows that the R_g's of the dendrimer−PEG5000 complexes reach apparent steady-state values at 50−100 ns. Autocorrelation functions for the radius of gyration, $C_{R_g}(t)$, yield relaxation times below ∼100 ns, defined as the time at which $C_{R_g}(t) = 1/e$, indicating that PEG5000-attached dendrimers are equilibrated within the simulated time scales. PEG550-attached dendrimers also showed a similar trend, although with a shorter equilibration time (data not shown). The R_g for the dendrimer−PEG5000 complex at neutral pH is 65.8 ± 1.7 Å, close to the value of 70.6 ± 2.8 Å obtained from SANS experiments.[48]

Figure 5 shows average end-to-end distances of PEG chains attached to dendrimer terminals. End-to-end distances of PEG550 covering 8−60 (i.e., 12−94%) of the dendrimer terminals are 17−18 Å, close to the end-to-end distance of 17.5 Å for a single free PEG550 chain in water from previous simulations.[33] This indicates that there is little effect of grafting on PEG550 chain conformation, even at high PEG-grafting density, presumably because PEG550 is not long enough to show an extended conformation. However, for grafted PEG5000 the end-to-end distance grows from 58 to 80 Å as the grafting density increases, which at high grafting density greatly exceeds the end-to-end distance of 56.3 Å for a single ungrafted PEG5000 in water. Thus, at higher PEG-grafting densities, PEG5000 chains have higher end-to-end distances, showing an extended "brush"-like conformation. The extended brush conformation was previously observed in simulations of PEG5000-attached dendrimers[18] and PEG2000 grafted on planar surface[33] using the same CG PEG model, in agreement with the brush−mushroom transition from the polymer theories.[49,50] For both PEG550 and PEG5000, the extent of protonation does not significantly influence the end-to-end distances of the PEG's.

To understand the effect of the PEG length and concentration on diffusivity of the dendrimer, diffusion coefficients (D) for the COM of dendrimer−PEGs were calculated. The slopes of the mean-square displacements (MSD) of the COM of dendrimer−PEGs versus time were calculated (D_{PBC}). Yeh and Hummer found that the diffusion coefficients increase as the system size increases because of the long-range interaction produced by the periodic boundary condition.[51] Therefore, D_{PBC} was corrected for finite size effects using the formula[51] $D = D_{PBC} + K_B T\xi/$

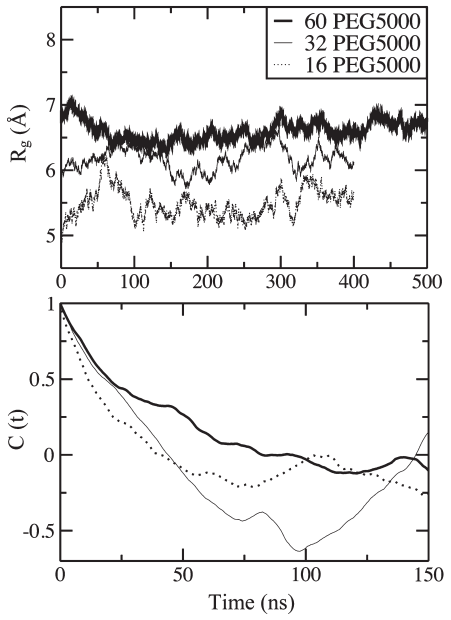

Figure 4. Radii of gyration (R_g, top) and autocorrelation function ($C(t)$, bottom) of R_g for G4 dendrimer−PEG5000 complexes (with 16, 32, and 60 copies of PEG5000 attached) at neutral pH.

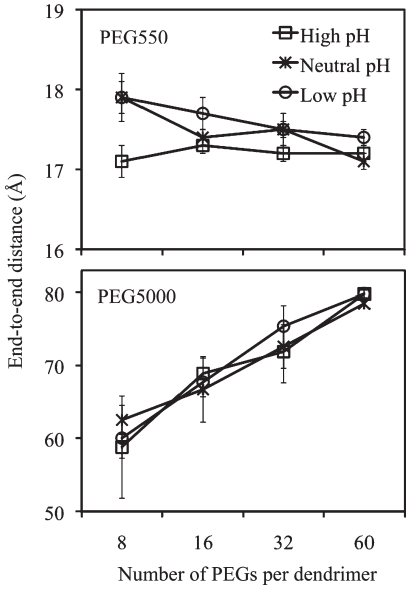

Figure 5. Average end-to-end distances of PEG chains grafted to terminal groups of the G4 dendrimer.

$6\pi\eta L$, where K_B is Boltzmann's constant, L is the cubic box length, $\xi = 2.837\,297$ (which has been found to be the coefficient for the correction factor for particles on a cubic lattice interacting electrostatically via Poisson's equation with Ewald summation),[52,53] and η is the viscosity of the medium ($\eta = 0.75$ cP at 298 K for CG water).[54] Note that $\eta = 0.75$ cP and $D = 1.92 \times 10^{-5}$ cm^2/s for CG water at 298 K, which are close to experimental values of 0.89 cP and 2.3×10^{-5} cm^2/s, indicating that diffusivity can be semiquantitatively predicted from the CG model. Figure 6 shows faster diffusivity for dendrimer−PEGs with smaller and fewer PEG chains.

Effect of PEGylation on Size and Internal Structure of the Dendrimer. The R_g values of the dendrimer portion of the dendrimer−PEG complex were calculated to determine the effect of PEGylation on the size of the dendrimer. Figure 7 shows that the dendrimer expands with increased PEG length and grafting density, although the size differences of the expanded dendrimers are small (1−3 Å). In Figure 8, the RDF for PEG beads show that the system with 60 chains of PEG5000 shows much higher PEG−PEG RDF's than do those with smaller or fewer chains, implying that the PEG's are crowded and hence force the dendrimer to expand to relieve PEG crowding. This has been also suggested by the experimental observation that there is more space to encapsulate hydrophobic compounds inside dendrimers with more PEG chains attached.[17] These results indicate that larger size and higher concentration of PEG induce swelling of the dendrimer.

To understand the effect of PEGylation on the internal structure of the dendrimer, radial densities of the dendrimer in the dendrimer−PEG complex were calculated. When plotted in Figure 9, these show that PEGylation yields a dense-shell structure at high and neutral pH, presumably because of dendrimer terminals stretched by PEG, as observed in Figure 7. However, dendrimers with 32 and 60 chains of PEG5000 show a much sharper peak at around 18−20 Å than do those with smaller or fewer chains, indicating a more dense shell structure for the former. A comparison of dense-core and dense-shell structures is visualized in Figure 10. These images show that there is a larger inner vacancy for the dendrimer with 32 PEG5000, compared to the dendrimer with 8 PEG5000, as is also inferred from their radial density distributions in Figure 9. These results indicate that longer chains and higher concentrations of PEG induce a more dense shell structure.

These simulation findings are consistent with the experiment observations regarding the effect of PEGylation on the solubility of hydrophobic pyrene in dendrimers. Experimentally, Yang et al. found that attachment of PEG750, PEG2000, or PEG5000 to 75% of the terminal groups of G3 PAMAM dendrimers increases the solubility of pyrene, presumably because the PEG chains stretch the dendrimer, leading to more space for the compound.[17] Encapsulation of more pyrene compounds (higher solubility of dendrimer−pyrene complexes) presumably requires a dense-shell structure with more space in the core. Therefore, this experimental observation is consistent with our simulations showing that attachment of PEG550 or PEG5000 swells the dendrimer due to formation of a dense-shell, expanded-core structure. However, experiments also showed that although PEG chains of all lengths increased the solubility of pyrene, the extent of solubility was not proportional to the size of PEG but was ordered such that solubility decreased in the order PEG2000 > PEG5000 > PEG750. This lower solubility with PEG5000 relative to PEG2000 was found even at low concentrations of dendrimer−PEGs. This was explained by the hypothesis that long PEG5000 chains may induce the interparticle aggregation of the dendrimer−PEG complexes, and in the aggregates the long PEG can penetrate into other dendrimer and partially occupy the inner cavity, leading to lower solubility of pyrene. However, our previous simulations showed that no aggregation is induced by either short PEG550 or long PEG5000 chains,[18] conflicting with this hypothesis.

To resolve this, cumulative numbers of PEG beads inside the dendrimer were calculated as a function of the radial distance from the center of the dendrimer. Figure 11 shows that the

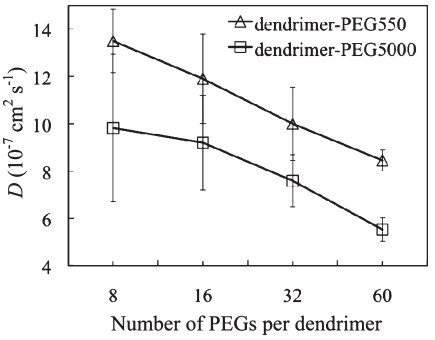

Figure 6. Diffusion coefficients D of centers of mass (COM) of dendrimer−PEGs at neutral pH.

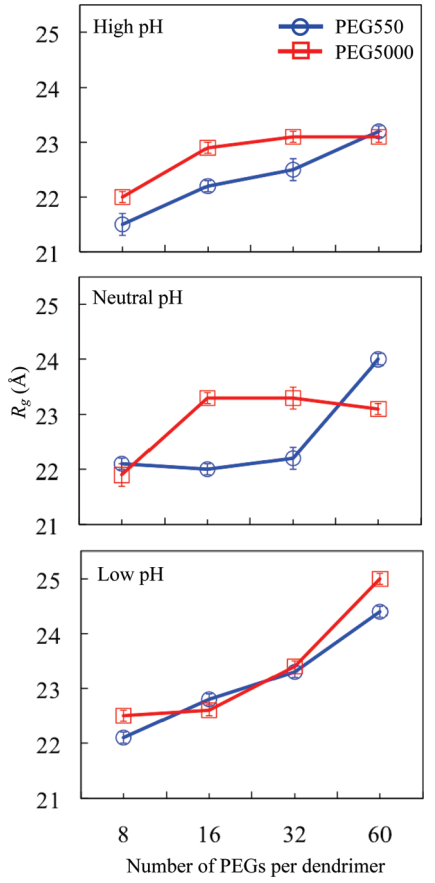

Figure 7. Average radii of gyration (R_g) of the dendrimer portion of the dendrimer−PEG complex.

highest cumulative numbers of PEG beads in the interior of the dendrimer are found for the systems with 16, 32, and 60 chains of PEG5000 at high and neutral pH. In particular, for dendrimers with 60 PEG5000 chains, there are ∼36 PEG beads within ∼10 Å from COM of the dendrimer, which encompasses the vacant interior where drug encapsulation occurs, indicating deep self-penetration of long PEG chains into their own dendrimer. For dendrimers with PEG550, very few PEG beads are found in the dendrimer interior, indicating that the PEG penetration is significantly affected by the PEG length. At low pH, for dendrimers with both PEG550 and PEG5000, very few PEG beads are found inside the dendrimer, presumably because cationic

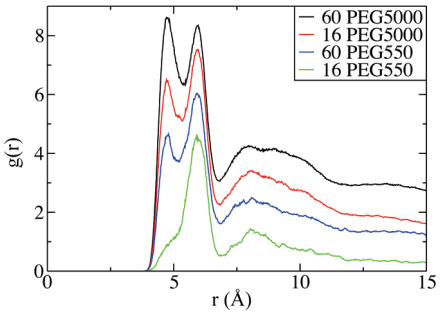

Figure 8. Radial distribution functions of PEG monomers in a dendrimer−PEG complex at neutral pH.

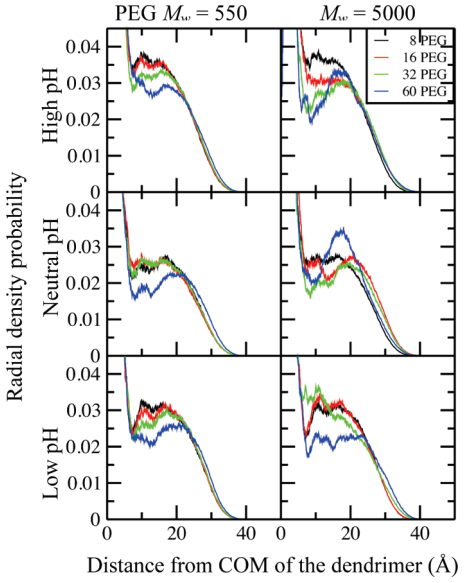

Figure 9. Radial density probabilities of the dendrimer in the dendrimer−PEG complex as a function of distance from center of mass (COM) of the dendrimer.

amines of the dendrimer interior tend to interact with anionic counterions or polar waters more strongly than with less-polar PEG chains, leading to more counterions and water instead of PEG inside the dendrimer. The long PEG-induced self-penetration can reduce the vacant interior and capability of encapsulating hydrophobic pyrenes, leading to lower solubility of pyrenes. These results imply that the experimental observation of lower solubility of pyrene for PEG5000 may be caused by the self-penetration of long PEG chains into dendrimers and not by the interparticle aggregation. It would obviously be interesting to simulate a PEGylated dendrimers in the presence of pyrene to determine whether or not long PEG's can indeed suppress pyrene encapsulation. However, such simulations would require either all-atom simulations of dendrimers with long PEG chains, which would be computationally very expensive, or the development of a CG model for pyrene, which would need to be validated. Both efforts, while worthwhile, are beyond the scope of this paper. Whether or not the results here can explain the unusual pyrene encapsulation experiments, we have shown that long dense PEG chains do penetrate into the cores of dendrimers, and this will certainly have implications for the ability of these nanoparticles to carry drug cargo into cells.

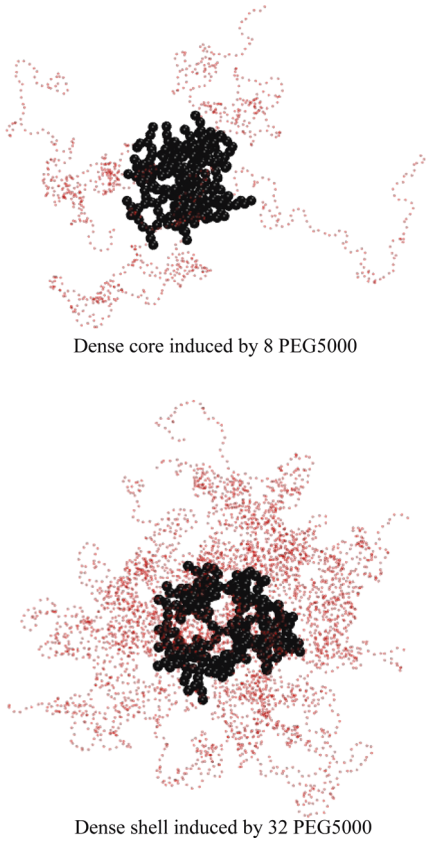

Figure 10. Snapshots of G4 dendrimers attached with 8 PEG5000 (top) and 32 PEG5000 (bottom) at the end of simulations, leading to dense-core and dense-shell structures, respectively. Black dots represent G4 dendrimer beads, and transparent red dots represent PEG5000. Water and ion beads are omitted for clarity. The images were created with VMD.[55]

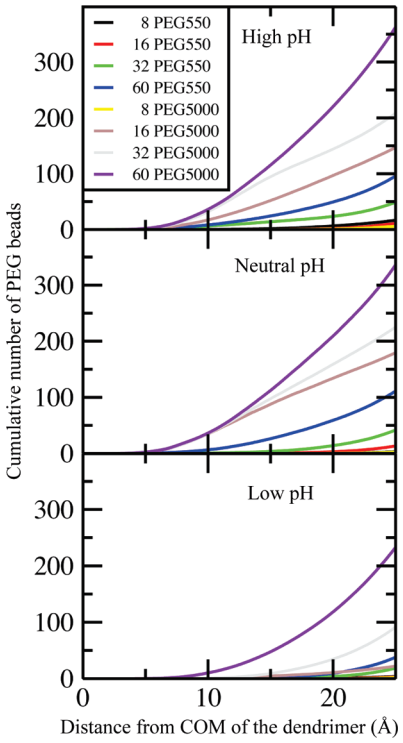

Figure 11. Cumulative number of PEG beads as a function of distance from the center of mass of the G4 dendrimer.

CONCLUSIONS

The CG PAMAM−dendrimer force field (FF) used in our earlier work was reparametrzied to better predict the radius of gyration R_g and the internal structure of dendrimers at different degrees of protonation, which is set by pH. While the previous CG dendrimer FF produced a ∼12% difference in the G5 dendrimer R_g values between high and neutral pH, the reparametrized FF shows only ∼4% difference, similar to that observed in recent SANS experiments.[31] The R_g values for G4, G5, and G7 dendrimers computed using the new FF agree well with those from experiments,[31] to within 4%. Simulations of unprotonated and protonated dendrimers show dense-core and dense-shell structures, respectively, similar to results from recent all-atom simulations,[32] indicating that the reparametrized CG FF can accurately predict both the sizes of dendrimers and their internal structures.

G4 PAMAM dendrimers functionalized with PEG's of different sizes (M_w = 550 and 5000) and grafting densities (8-, 16-, 32-, and 60-PEG chains) were simulated using the previously developed CG PEG[33] and reparametrized CG dendrimer FFs. The R_g value of the fully PEG5000-attached G4 dendrimer at neutral pH from the simulation is 65.8 ± 1.7 Å, close to the value of 70.6 ± 2.8 Å measured in a SANS experiment.[48] We find that PEG5000 chains are extended in a brush at high grafting density, while PEG550 chains are not, presumably because PEG550 is too short to extend much even at high grafting density. Diffusivities for PEG5000-attached dendrimers were found to be slower than those for PEG550-attached dendrimers.

Dendrimers grafted with larger PEG's at higher grafting densities showed larger R_g and denser dendrimer shell structure. This effect of the PEG size and grafting density is consistent with experimental measurements of the solubility of a small hydrophobic compound in the PEGylated dendrimer, which showed increases in solubility with increased PEG size up to PEG2000. However, experiments also showed a decrease in solubility when the PEG size was increased further to PEG5000. To explain this nonmonotonic effect, it has been hypothesized that long PEG chains induce interparticle aggregation, whereby PEG chains can penetrate into other dendrimers and thus suppress uptake of a hydrophobic compound.[17] However, our previous simulations showed no interparticle aggregation, while our new simulations show that long PEG5000 chains at high grafting density self-penetrate into the attached dendrimer, occupying the dendrimer's vacant interior that would otherwise be available for encapsulating hydrophobic compounds. These results suggest that the observed lower uptake with PEG5000 might be induced by self-penetration of PEG chains into their own dendrimers, not by the interparticle aggregation.

AUTHOR INFORMATION

Corresponding Author

*E-mail: leeh@dankook.ac.kr.

REFERENCES

(1) Astruc, D.; Boisselier, E.; Ornelas, C. *Chem. Rev.* **2010**, *110*, 1857–1959.

(2) Majoros, I. J.; Keszler, B.; Woehler, S.; Bull, T.; Baker, J. R. *Macromolecules* **2003**, *36*, 5526–5529.
(3) Majoros, I. J.; Williams, C. R.; Baker, J. R. *Curr. Top. Med. Chem.* **2008**, *8*, 1165–1179.
(4) Malik, N.; Evagorou, E. G.; Duncan, R. *Anti-Cancer Drugs* **1999**, *10*, 767–776.
(5) Menjoge, A. R.; Kannan, R. M.; Tomalia, D. A. *Drug Discov. Today* **2010**, *15*, 171–185.
(6) Patri, A. K.; Kukowska-Latallo, J. F.; Baker, J. R. *Adv. Drug Delivery Rev.* **2005**, *57*, 2203–2214.
(7) Sarkar, K.; Yang, H. *Drug Delivery* **2008**, *15*, 343–346.
(8) Svenson, S. *Eur. J. Pharm. Biopharm.* **2009**, *71*, 445–462.
(9) Tekade, R. K.; Kumar, P. V.; Jain, N. K. *Chem. Rev.* **2009**, *109*, 49–87.
(10) Harris, J. M.; Chess, R. B. *Nat. Rev. Drug Discov.* **2003**, *2*, 214–221.
(11) Harris, J. M.; Martin, N. E.; Modi, M. *Clin. Pharmacokinet.* **2001**, *40*, 539–551.
(12) Bhadra, D.; Bhadra, S.; Jain, S.; Jain, N. K. *Int. J. Pharm.* **2003**, *257*, 111–124.
(13) Gupta, U.; Agashe, H. B.; Asthana, A.; Jain, N. K. *Biomacromolecules* **2006**, *7*, 649–658.
(14) Huang, R. Q.; Qu, Y. H.; Ke, W. L.; Zhu, J. H.; Pei, Y. Y.; Jiang, C. *FASEB J.* **2007**, *21*, 1117–1125.
(15) Kojima, C.; Toi, Y.; Harada, A.; Kono, K. *Bioconjugate Chem.* **2007**, *18*, 663–670.
(16) Kim, Y.; Klutz, A. M.; Jacobson, K. A. *Bioconjugate Chem.* **2008**, *19*, 1660–1672.
(17) Yang, H.; Morris, J. J.; Lopina, S. T. *J. Colloid Interface Sci.* **2004**, *273*, 148–154.
(18) Lee, H.; Larson, R. G. *J. Phys. Chem. B* **2009**, *113*, 13202–13207.
(19) Kelly, C. V.; Leroueil, P. R.; Nett, E. K.; Wereszczynski, J. M.; Baker, J. R.; Orr, B. G.; Holl, M. M. B.; Andricioaei, I. *J. Phys. Chem. B* **2008**, *112*, 9337–9345.
(20) Kelly, C. V.; Leroueil, P. R.; Orr, B. G.; Holl, M. M. B.; Andricioaei, I. *J. Phys. Chem. B* **2008**, *112*, 9346–9353.
(21) Tanis, I.; Karatasos, K. *Phys. Chem. Chem. Phys.* **2009**, *11*, 10017–10028.
(22) Carbone, P.; Negri, F.; Muller-Plathe, F. *Macromolecules* **2007**, *40*, 7044–7055.
(23) Lee, H.; Larson, R. G. *J. Phys. Chem. B* **2006**, *110*, 18204–18211.
(24) Lee, H.; Larson, R. G. *J. Phys. Chem. B* **2008**, *112*, 7778–7784.
(25) Lee, H.; Larson, R. G. *J. Phys. Chem. B* **2008**, *112*, 12279–12285.
(26) Lee, H.; Larson, R. G. *Molecules* **2009**, *14*, 423–438.
(27) Hess, B.; Kutzner, C.; van der Spoel, D.; Lindahl, E. *J. Chem. Theory Comput.* **2008**, *4*, 435–447.
(28) Lindahl, E.; Hess, B.; van der Spoel, D. *J. Mol. Model.* **2001**, *7*, 306–317.
(29) Marrink, S. J.; de Vries, A. H.; Mark, A. E. *J. Phys. Chem. B* **2004**, *108*, 750–760.
(30) Marrink, S. J.; Risselada, H. J.; Yefimov, S.; Tieleman, D. P.; de Vries, A. H. *J. Phys. Chem. B* **2007**, *111*, 7812–7824.
(31) Liu, Y.; Chen, C. Y.; Chen, H. L.; Hong, K. L.; Shew, C. Y.; Li, X.; Liu, L.; Melnichenko, Y. B.; Smith, G. S.; Herwig, K. W.; Porcar, L.; Chen, W. R. *J. Phys. Chem. Lett.* **2010**, *1*, 2020–2024.
(32) Liu, Y.; Bryantsev, V. S.; Diallo, M. S.; Goddard, W. A. *J. Am. Chem. Soc.* **2009**, *131*, 2798–2799.
(33) Lee, H.; de Vries, A. H.; Marrink, S. J.; Pastor, R. W. *J. Phys. Chem. B* **2009**, *113*, 13186–13194.
(34) Lee, H.; Venable, R. M.; MacKerell, A. D.; Pastor, R. W. *Biophys. J.* **2008**, *95*, 1590–1599.
(35) Berendsen, H. J. C.; Postma, J. P. M.; van Gunsteren, W. F.; DiNola, A.; Haak, J. R. *J. Chem. Phys.* **1984**, *81*, 3684–3690.
(36) Essmann, U.; Perera, L.; Berkowitz, M. L.; Darden, T.; Lee, H.; Pedersen, L. G. *J. Chem. Phys.* **1995**, *103*, 8577–8593.
(37) Lin, S. T.; Maiti, P. K.; Goddard, W. A. *J. Phys. Chem. B* **2005**, *109*, 8663–8672.
(38) Maiti, P. K.; Cagin, T.; Lin, S. T.; Goddard, W. A. *Macromolecules* **2005**, *38*, 979–991.
(39) Maiti, P. K.; Goddard, W. A. *J. Phys. Chem. B* **2006**, *110*, 25628–25632.
(40) Blaak, R.; Lehmann, S.; Likos, C. N. *Macromolecules* **2008**, *41*, 4452–4458.
(41) Lee, I.; Athey, B. D.; Wetzel, A. W.; Meixner, W.; Baker, J. R. *Macromolecules* **2002**, *35*, 4510–4520.
(42) Welch, P.; Muthukumar, M. *Macromolecules* **1998**, *31*, 5892–5897.
(43) Chen, W. R.; Porcar, L.; Liu, Y.; Butler, P. D.; Magid, L. J. *Macromolecules* **2007**, *40*, 5887–5898.
(44) Li, T. F.; Hong, K.; Porcar, L.; Verduzco, R.; Butler, P. D.; Smith, G. S.; Liu, Y.; Chen, W. R. *Macromolecules* **2008**, *41*, 8916–8920.
(45) Porcar, L.; Hong, K. L.; Butler, P. D.; Herwig, K. W.; Smith, G. S.; Liu, Y.; Chen, W. R. *J. Phys. Chem. B* **2010**, *114*, 1751–1756.
(46) Porcar, L.; Liu, Y.; Verduzco, R.; Hong, K. L.; Butler, P. D.; Magid, L. J.; Smith, G. S.; Chen, W. R. *J. Phys. Chem. B* **2008**, *112*, 14772–14778.
(47) Lee, H.; Baker, J. R.; Larson, R. G. *J. Phys. Chem. B* **2006**, *110*, 4014–4019.
(48) Hedden, R. C.; Bauer, B. J. *Macromolecules* **2003**, *36*, 1829–1835.
(49) de Gennes, P. G. *Adv. Colloid Interface Sci.* **1987**, *27*, 189–209.
(50) Vagberg, L. J. M.; Cogan, K. A.; Gast, A. P. *Macromolecules* **1991**, *24*, 1670–1677.
(51) Yeh, I. C.; Hummer, G. *J. Phys. Chem. B* **2004**, *108*, 15873–15879.
(52) Nijboer, B. R. A.; Ruijgrok, T. W. *J. Stat. Phys.* **1988**, *53*, 361–382.
(53) Cichocki, B.; Felderhof, B. U.; Hinsen, K. *Phys. Rev. A* **1989**, *39*, 5350–5358.
(54) Fuhrmans, M.; Sanders, B. P.; Marrink, S. J.; de Vries, A. H. *Theor. Chem. Acc.* **2009**, *125*, 335–344.
(55) Humphrey, W.; Dalke, A.; Schulten, K. *J. Mol. Graphics* **1996**, *14*, 33–38.